SCIENTIA
Series A: *Mathematical Sciences*, Vol. 13 (2006), 22–35
Universidad Técnica Federico Santa María
Valparaíso, Chile
ISSN 0716-8446

A multiresolution finite difference scheme for spatially one-dimensional strongly degenerate parabolic equations

Raimund Bürger[A], Alice Kozakevicius[B] and Mauricio Sepúlveda[A]

Abstract. An adaptive finite difference method for one-dimensional strongly degenerate parabolic equations is presented. Using an explicit conservative numerical scheme with a third-order Runge-Kutta method for the time discretization, a third-order ENO interpolation for the convective term, and adding a conservative discretization for the diffusive term, we apply the multiresolution method combining the switch between central interpolation or exact computing of numerical flux, and a wavelet transform applied to point values of the solution to control the switch. Applications to mathematical models of sedimentation-consolidation processes and traffic flow with driver reaction illustrate the new method.

1. Introduction

1.1. Scope. High resolution schemes for conservation laws are of at least second-order accuracy wherever the solution is smooth, and on the other hand resolve discontinuities sharply and without spurious oscillations. The multiresolution method has been devised (at least, originally) to reduce the computational cost of high resolution methods. In standard situations, the solution u of the conservation law

$$u_t + f(u)_x = 0, \quad (x,t) \in Q_T := \Omega \times [0,T], \quad \Omega \subseteq \mathbb{R} \tag{1.1}$$

exhibits strong variations (shocks) in small regions but behaves smoothly on the major portion of Q_T. The multiresolution technique adaptively concentrates computational effort on the regions of strong variation. It goes back to Harten [**15**] for hyperbolic equations and was used by Bihari [**2**] and Roussel et al. [**21**] for parabolic equations. Multiresolution methods for conservation laws in several space dimensions are analyzed in [**12**], while fully adaptive multiresolution finite volume schemes, including an optimized adaptive memory storage, are presented in [**11, 21**].

2000 *Mathematics Subject Classification.* Primary 35K65 Secondary 65M06.
Key words and phrases. Multiresolution schemes, strongly degenerate parabolic equations, ENO interpolation, thresholded wavelet transform, thresholding strategy.

In this note we construct adaptive multiresolution schemes, and present numerical experiments, for strongly degenerate parabolic equations of the type

$$u_t + f(u)_x = A(u)_{xx}, \quad (x,t) \in Q_T, \tag{1.2}$$

where we assume that the functions $f, A : \mathbb{R} \to \mathbb{R}$ are piecewise smooth and Lipschitz continuous, and that $A(v) \geqslant A(u)$ for $v > u$. We admit intervals $[\alpha, \beta]$ with $A(u) =$ const., such that (1.2) degenerates into the first-order conservation law $u_t + f(u)_x = 0$ for all $u \in [\alpha, \beta]$. If there is at least one such u-interval of positive length, (1.2) is called *strongly degenerate*. In that case, solutions of (1.2) are in general discontinuous, and need to be characterized as weak solutions along with an entropy condition to select the physically relevant *entropy solution*. Applications of (1.2) include models of sedimentation-consolidation processes [**1, 6**], two-phase flow in porous media [**13**], and traffic flow with driver reaction [**8**].

1.2. Multiresolution schemes. Suppose that we are given a conservative high-resolution scheme on a uniform mesh for the solution of (1.1) or (1.2). Then the multiresolution method approximates the solution to a given tolerance in a more efficient way, where by gain of efficiency we understand a reduction of the number of exact flux evaluations required by the high-resolution scheme. To this purpose, point values or cell averages of the numerical solution are defined on a hierarchical sequence of nested diadic meshes, where the initially given mesh is the finest one of the sequence. The multiresolution representation of the numerical solution consists of its grid averages for the coarsest grid and the set of errors for predicting the grid averages of each resolution level in this hierarchy from those of the next coarsest one. The same kind of multiresolution representation can be obtained for point values of the solution. The information contained in the multiresolution analysis of the numerical solution is used to locate discontinuities, since a wavelet coefficient takes into account the regularity of a function in each position and on each scale. This idea was exploited first by Harten [**14, 15, 16**] for solving hyperbolic conservations laws. He designed a sensor to decide at which positions of a fine mesh the flux should be exactly evaluated, and where otherwise it can be obtained more cheaply by interpolation of pre-calculated fluxes on coarser scales. Roughly speaking, small multiresolution coefficients at a given level indicate areas where the solution is smooth, and fluxes may thus be obtained by interpolation; otherwise, they need to be evaluated exactly. The criterion whether a multiresolution coefficient (also called *wavelet coefficient* or *detail*) is 'small' is defined by comparing its absolute value with a level-dependent *threshold* value. There are many different so-called *strategies* of introducing threshold values for each grid level.

Additional efficiency can be gained through data compression by a *hard thresholding* or *truncation* operation. This means that one not only tests whether a multiresolution coefficient is small compared to a threshold value in order to decide whether its position is significant, but that one indeed sets a small coefficient to zero to attain data compression. We herein only use thresholding to determine significant positions in the sense of Harten, and do not use hard thresholding or calculate an SPR, but focus on attaining a smaller number of exact flux evaluations.

To solve strongly degenerate parabolic equations, we herein combine two basic concepts to obtain a multiresolution scheme: firstly, the switch between central interpolation of both convective and diffusive parts of the numerical flux and an ENO reconstruction of the convective flux combined with a finite difference of explicit evaluations of the integrated diffusion function $A(u)$, and secondly, a wavelet transform applied to point values of the solution to control the switch. The first alternative of the switch is performed on smooth portions of the solution, while the second applies near strong variations. To maintain overall second order accuracy both in x and t without creating spurious oscillations, we use a third-order TVD-Runge-Kutta scheme [**22**] for the time evolution of the solution.

Although our treatment is spatially one-dimensional, the multiresolution scheme can be extended to two or more dimensions by a bidimensional wavelet transform involving a tensor product approach, and by interpolating the numerical divergence from coarser to finer levels [**3**]. One may also keep the interpolatory framework as in the one-dimensional case, but split the divergence by directions [**10, 17**].

1.3. Initial and boundary conditions. We consider the zero-flux initial-boundary value problem for a bounded domain $\Omega := [0, L]$ with the conditions

$$u(x,0) = u_0(x), \quad x \in \Omega; \quad f(u) - A(u)_x = 0 \quad \text{on } \partial\Omega = \{0, L\},\ t \in (0, T]. \tag{1.3}$$

In [**6**] existence and uniqueness of BV entropy solutions to (1.2), (1.3) is shown. On the other hand, the convergence of monotone schemes for (1.2), (1.3) is proved in [**5**]. The scheme developed herein is, however, not monotone in general.

2. The multiresolution scheme

2.1. Multiresolution framework. Let $(G^0, G^1, \dots, G^{L_c})$ denote a family of uniform nested grids on the interval $I := [a, b]$, where $G^0 := (x_0^0, x_1^0, \dots, x_{N_0}^0)$, $N_0 = 2^m$, $m \in \mathbb{N}$ is the finest one (the finest resolution level), and $h_0 := (b-a)/N_0$ is the finest cell length. The values of a function u on G^0 are the input data. The remaining diadically coarsened grids are obtained in the following recursive way: given a grid G^{k-1}, we obtain the next coarsest grid G^k by removing the even-indexed grid points. Therefore $G^{k-1} \setminus G^k = (x_{2j-1}^{k-1})_{j=1,\dots,N_k}$, $G^{k-1} \cap G^k = G^k$, and $x_j^k = x_{2j}^{k-1}$ for $0 \leqslant j \leqslant N_k = 2^{m-k}$, $k = 1, \dots, L_c$. Due to the embedding of the grids, the representation of u on any coarser grid G^k, $k = 1, \dots, L_c$ can be obtained directly from the finest level $k = 0$: $u_j^k = u(x_j^k) = u(x_{2^k j}^0) = u_{2^k j}^0$ for $0 \leqslant j \leqslant N_k$. To recover the representation of u on G^{k-1} from its representation on the next coarser grid G^k, we need an interpolation operator $\mathcal{I}(u^k, x)$ of u on G^k to obtain approximations for the missing points of G^{k-1}. The function value at x_{2j-1}^{k-1} is obtained from the $(r-1)$-th degree polynomial interpolating the $r = 2s$ consecutive points $(u_{j-s}^k, \dots, u_{j+s-1}^k)$. Therefore

$$\tilde{u}_{2j-1}^{k-1} = \mathcal{I}\big(u^k, x_{2j-1}^{k-1}\big) = \sum_{l=1}^{s} \beta_l \big(u_{j+l-1}^k + u_{j-l}^k\big), \quad r = 2s, \tag{2.1}$$

with $\beta_1 = 1/2$ for $r = 2$ and $\beta_1 = 9/16$, $\beta_2 = -1/16$ for $r = 4$. The interpolation errors, known as *details* or *wavelet coefficients*, are $d_j^k = u_{2j-1}^{k-1} - \tilde{u}_{2j-1}^{k-1}$ for $1 \leqslant j \leqslant N_k$.

Thus, with the knowledge of $u^k := (u_0^k, u_1^k, \ldots, u_{N_k}^k)$ and $d^k := (d_0^k, d_1^k, \ldots, d_{N_k}^k)$, we can exactly recover the representation of u on G^{k-1}. The pair of vectors (u^k, d^k) is the *multiresolution representation* of u^{k-1}. Applying successively this procedure for $1 \leqslant k \leqslant L_c$, we can recover the values of u on the finest level of resolution from its values on the coarsest level L_c and the sequence of all details from levels L_c to 1:

$$u^0 \leftrightarrow (d^1, u^1) \leftrightarrow (d^1, d^2, u^2) \leftrightarrow \cdots \leftrightarrow (d^1, d^2, \ldots, d^{L_c}, u^{L_c}) =: u_{\mathrm{M}}, \tag{2.2}$$

where u_{M} is the *multiresolution representation* of $u^0 \equiv u$. The details d^k contain information on the smoothness of u, and will be used to flag the non-smooth parts of the solution in the adaptive numerical method.

Note that we explicitly regard the solution values as pointwise values, and that our scheme is a finite difference scheme. An alternative treatment would be to consider solution values as cell averages, and to derive a corresponding multiresolution finite volume scheme, see [**9**].

2.2. Regularity analysis and data compression. Away from discontinuities of u, the wavelet coefficients d_j^k diminish in size as the levels of resolution become finer, at a rate which is determined by the local regularity of u and the order of accuracy of the approximation.

We see that in the neighborhood of a discontinuity of the function, the wavelet coefficients remain of the same size for all levels of refinement. This observation is used here only for the construction of the set $\mathcal{D}^n$ of significant positions. Roughly speaking, if d_j^k are the details of the multiresolution representation of the fine-grid solution u^n and time t_n, then the significant positions for the next time step could be defined as the those points x_j^k for which $(j,k) \in \mathcal{D}^n$, where

$$\mathcal{D}^n = \big\{(j,k)\big|\ \big|d_j^k\big| \geqslant \varepsilon_k, 1 \leqslant j \leqslant N_k, 1 \leqslant k \leqslant N_c\big\}, \tag{2.3}$$

where $\varepsilon_k = 2^{k-L_c}\varepsilon$ (see [**17**]). Finally, the index set of significant coefficients in each time step has to capture the finite speed of propagation of information and the formation of shock waves. For this reason, Harten [**15**] proposed an algorithm to extend $\mathcal{D}^n$ after thresholding, including so-called *safety points* near positions associated with significant details, which yields an extended index set $\tilde{\mathcal{D}}^n$. In order to solve strongly degenerate parabolic equations we also need to include safety points at the same level of the respective significant details (for the transport of information) and points on a higher level than the significant detail (for shock capturing). We determine $\tilde{\mathcal{D}}^n$ by a similar version of Harten's algorithm [**15**, Algorithm (6.1)].

2.3. Time and space discretization. For the time discretization of the sample equation

$$u_t = \mathcal{L}(u) \equiv -f(u)_x + A(u)_{xx}, \quad (x,t) \in Q_T := \Omega \times [0,T], \quad \Omega = [0,1]. \tag{2.4}$$

we use an explicit Runge-Kutta TVD scheme of third order [**22**].

Point values of the initial solution of (1.1) are given in an uniform fine grid G^0, $u_i = u(x_i)$, and the extended index set of significant multiresolution coefficients, $\tilde{\mathcal{D}}^0$, is considered already built. Furthermore, let us recall that the unknown u_j^n, actually represents an average taken over a cell of length Δx centered at the fine-grid position

x_j. Thus, the numerical fluxes that determine the evolution of u_j^n are associated with the cell boundaries located at $x_j - \Delta x/2$ and $x_j + \Delta x/2$, and are therefore indexed by $j-1/2$ and $j+1/2$, respectively. Let $du_j(t)/dt = \mathcal{L}_j(u(t))$, where $u(t) := (u_0(t), \ldots, u_{N_0}(t))$ and $\mathcal{L}_j(u)$ contains the flux and diffusion terms. We limit here the discussion to the zero-flux initial-boundary value problem (1.2), (1.3); in this case it is convenient to distinguish between the interior operators $\mathcal{L}_1, \ldots, \mathcal{L}_{N_0-1}$ and the boundary operators $\mathcal{L}_0$ and $\mathcal{L}_{N_0}$, which result from including the boundary conditions in the fully discrete version. For this initial-boundary value problem, a conservative semi-discrete scheme is given by

$$\bar{\mathcal{L}}_j\big(u(t)\big) := \frac{1}{\Delta x}\begin{cases} -\big(\bar{F}_{1/2} - \bar{D}_{1/2}\big), & j = 0, \\ -\big(\bar{F}_{j+1/2} - \bar{F}_{j-1/2} - (\bar{D}_{j+1/2} - \bar{D}_{j-1/2})\big), & j = 1, \ldots, N_0, \\ \big(\bar{F}_{N_0-1/2} - \bar{D}_{N_0-1/2}\big), & j = N_0 + 1, \end{cases}$$

where the numerical fluxes $\bar{F}_{i+1/2}$ and $\bar{D}_{i+1/2}$ contain the advective and diffusive terms, respectively.

If $i \in \tilde{\mathcal{D}}^n$, then we use a Lax-Friedrichs splitting [**22**] with a third-order ENO interpolation for $\bar{F}_{i+1/2}$, in agreement with the order of the TVD Runge-Kutta scheme, and add a fine-grid finite difference of the diffusion term. On the other hand, if $i \notin \tilde{\mathcal{D}}^n$, the numerical flux is no longer evaluated exactly; instead, it is approximated by centred interpolation of fluxes previously evaluated on a coarser level. By construction, all positions from the coarsest level, L_c, of the multiresolution representation of u^n are in $\tilde{\mathcal{D}}^n$. Therefore all fluxes on level L_c are exactly evaluated in each time step n. The u-values required for the flux computation are taken from the finest level, $k = 0$.

The diffusive fluxes at level k are calculated by

$$D_{i+1/2}^k := \frac{1}{\Delta x}\left(A\big(u_{2^k i+1}^0\big) - A\big(u_{2^k i}^0\big)\right). \tag{2.5}$$

Since the ENO interpolator needs six points to search the least oscillatory four-point stencil for the flux calculation, it is necessary to extrapolate the solution across the boundaries of I in order to compute the extra flux values in the vicinities of x_0 and x_{N_0}. According to (1.3) we consider a linear extrapolation at the left boundary and a constant extrapolation at the right one, keeping the finest grid spacing.

For an interpolator in the non-periodic case, we have to modify the filters introduced in (2.1) for the first and the last points inside the stencil.

2.4. Numerical stability. The time step Δt is the same for all scales in the multiresolution, so the stability condition is the same as that of the finite difference scheme on the finest grid. According to [**7**], the CFL condition is given by

$$\mathrm{CFL} = \max_u |f'(u)|\frac{\Delta t}{\Delta x} + 2\max_u |a(u)|\frac{\Delta t}{(\Delta x)^2} \leqslant 1. \tag{2.6}$$

Once the multiresolution of u^n is given, all intermediate steps of the time evolution scheme will consider the same set $\tilde{\mathcal{D}}^n$. Now we summarize all described steps, presenting the following algorithm:

2.5. Multiresolution algorithm. We present the multiresolution scheme as an operation on the given finest grid, in which numerical fluxes of the given scheme are computed within a prescribed tolerance by a combination of direct flux evaluation and interpolation. We calculate the approximate solutions $u^{n,0}$, $n = 1, \dots, \mathcal{N}$, where $\mathcal{N}$ is the number of time steps, by the following sequence of operations:

ALGORITHM 2.1.

1. *Create the initial set of significant positions and define* $\tilde{\mathcal{D}}^0$. *As* $u_j = u_0(x_j)$, $j = 0, \dots, N_0$ *are point values, there is no need to compute the entire multiresolution representation.*
2. *For all the time step* $n = 1, \dots, \mathcal{N}$
   a) *For all the space discretization of the fine grid* $j = 0, \dots, N_0$, *for* $i = 1, \dots, n_{\mathrm{RK}}$ *and for* $k = 0, \dots, i-1$, *using* $u_0^{(k)}, \dots, u_{N_0}^{(k)}$ *as input data on* G^0, *calculate* $\bar{\mathcal{L}}_j(u^{(k)})$ *computing fluxes for all the levels: using Lax-Friedrichs splitting scheme and explicit formula if* $\hat{\imath}(j,k) = 1$, *and else using centered Lagrangean interpolator.*
   b) $u_j^{(i)} \leftarrow \sum_{k=0}^{i-1} \Big(\alpha_{ik} u_j^{(k)} + \Delta t \beta_{ik} \bar{\mathcal{L}}_j\big(u^{(k)}\big) \Big), \quad j = 0, \dots, N_0.$
   c) $u_j^{n+1,0} \leftarrow u_j^{(n_{\mathrm{RK}})}$ *for* $j = 0, \dots, N_0$, *compute the multiresolution representation of* $u^{n+1,0}$, *calculate the new set* $\tilde{\mathcal{D}}^{n+1}$.

2.6. Other boundary conditions. For periodic boundary conditions we do not need separate formulae for $\bar{\mathcal{L}}_0$ and $\bar{\mathcal{L}}_{N_0}$, since $\bar{\mathcal{L}}_j$ can always be computed from the interior formula of Lagrangean interpolation if we identify u_{N+s} with u_s, $s = 1, 2, 3, \dots$. Moreover, no extrapolation is needed to compute the ENO interpolation and the filters for the Lagrangean interpolation are always for the centered stencil. For our examples of initial-value problems, however, the computational domain has been chosen large enough so that the solution never reaches its boundary, so Algorithm 2.1 effectively also handles initial-value problems.

3. Applications of strongly degenerate parabolic equations

3.1. Sedimentation-consolidation processes. We limit ourselves here to one-dimensional batch settling of a suspension of initial concentration $u_0 = u_0(x)$ in a column of height L, where $u_0(x) \in [0, u_{\max}]$ and $u_{\max}$ is a maximum solids volume fraction. The relevant initial-boundary value problem is (1.2), (1.3). The unknown is the solids concentration u as a function of time t and depth x. The material specific behaviour of the suspension is characterized by the hindered settling function $f(u)$ and the integrated diffusion coefficient $A(u)$, which models the sediment compressibility. The function $f(u)$ is assumed to be continuous and piecewise smooth with $f(u) > 0$ for $u \in (0, u_{\max})$ and $f(u) = 0$ for $u \leqslant 0$ and $u \geqslant u_{\max}$. A typical example is

$$f(u) = \begin{cases} v_\infty u(1-u)^C & \text{for } u \in (0, u_{\max}), \\ 0 & \text{otherwise,} \end{cases} \qquad v_\infty > 0, \quad C > 0, \tag{3.1}$$

where $v_\infty > 0$ is the Stokes velocity, i.e., the settling velocity of a single particle in unbounded fluid. Moreover, we assume that $A(u) = \int_0^u a(s)\, ds$, $a(u) := f(u)\sigma_{\mathrm{e}}'(u)/(\Delta_\varrho g u)$,

where $\Delta_\varrho > 0$ is the solid-fluid density difference, g is the acceleration of gravity, and $\sigma_{\mathrm{e}}'(u)$ is the derivative of the material specific effective solid stress function $\sigma_{\mathrm{e}}(u)$. We assume that the solid particles touch each other at a critical concentration value (or gel point) $0 \leqslant u_{\mathrm{c}} \leqslant u_{\max}$, and that $\sigma_{\mathrm{e}}(u), \sigma_{\mathrm{e}}'(u) = 0$ for $u \leqslant u_{\mathrm{c}}$ and $\sigma_{\mathrm{e}}(u), \sigma_{\mathrm{e}}'(u) > 0$ for $u > u_{\mathrm{c}}$. This implies that $a(u) = 0$ for $u \leqslant u_{\mathrm{c}}$, such that this application motivates an equation of the type (1.2) that is indeed strongly degenerate parabolic. A typical function is

$$\sigma_{\mathrm{e}}(u) = 0 \text{ for } u \leqslant u_{\mathrm{c}}, \quad \sigma_{\mathrm{e}}(u) = \sigma_0[(u/u_{\mathrm{c}})^\beta - 1] \text{ for } u > u_{\mathrm{c}},\ \sigma_0 > 0,\ \beta > 1. \tag{3.2}$$

3.2. Traffic flow with driver reaction. The classic Lighthill-Whitham-Richards (LWR) kinematic wave model [**18, 20**] for unidirectional traffic flow on a single-lane highway starts from the principle of "conservation of cars" with a hiperbolic equation (1.1) where u is the density of cars as a function of distance x and time t and $f(u) = uv$, with $v = v(x,t)$ the velocity of the car located at position x at time t. The decisive constitutive assumption of the LWR model is that v is a function of u only, $v = v(u)$. We here use the Dick-Greenberg model [**8**]

$$V(u) = V_2(u) := \min\{1, C\ln(u_{\max}/u)\}, \quad C > 0. \tag{3.3}$$

We employ the diffusively corrected kinematic wave model (DCKWM), which extends the LWR model by a diffusion term that accounts for the drivers' anticipation length and reaction time. The result is a strongly degenerate parabolic convection-diffusion equation. The DCKWM model is based on the standpoint that a more realistic model than the LWR model should incorporate a reaction time τ, representing drivers' delay in their response to events, and drivers adjust their velocity to the density seen an anticipating distance L_a ahead. The DCKWM model is given by (1.2), where $A(u) := \int_0^u a(s)\,ds$, with

$$a(u) := \begin{cases} 0 & \text{if } u \leqslant u_{\mathrm{c}}, \\ -uv_{\max}V'(u)\big(L_a(u) + \tau v_{\max} u V'(u)\big) & \text{if } u > u_{\mathrm{c}}, \end{cases} \tag{3.4}$$

see [**8**] for details. There are at least two motivations for a critical density u_{c}. One of them is based on the Dick-Greenberg model (3.3); obviously, $V_2'(u) = 0$ for $u \leqslant u_{\mathrm{c}} := u_{\max}\exp(-1/C)$, so that (3.4) is satisfied for $V(u) = V_2(u)$. A more general viewpoint is that u_{c} is a threshold value for driver reaction. Both motivations give rise to the same behaviour of the diffusion coefficient. Moreover, we assume that $V(u)$ is chosen such that $\tilde{D}'(u) > 0$ for $u_{\mathrm{c}} < u < u_{\max}$. Consequently, the right-hand side of (1.2) vanishes on the interval $[0, u_{\mathrm{c}}]$, and possibly at the maximum density $u_{\max}$. Finally, we point out that Nelson [**19**] suggests a dependence $L_a = L_a(v(u))$ of the following type:

$$L_a = \max\big\{(v(u))^2/(2a), L_{\min}\big\}, \tag{3.5}$$

where the first argument is the distance required to decelerate to full stop from speed $v(u)$ at deceleration a, and the second imposes a minimal anticipation distance, regardless of how small the velocity is.

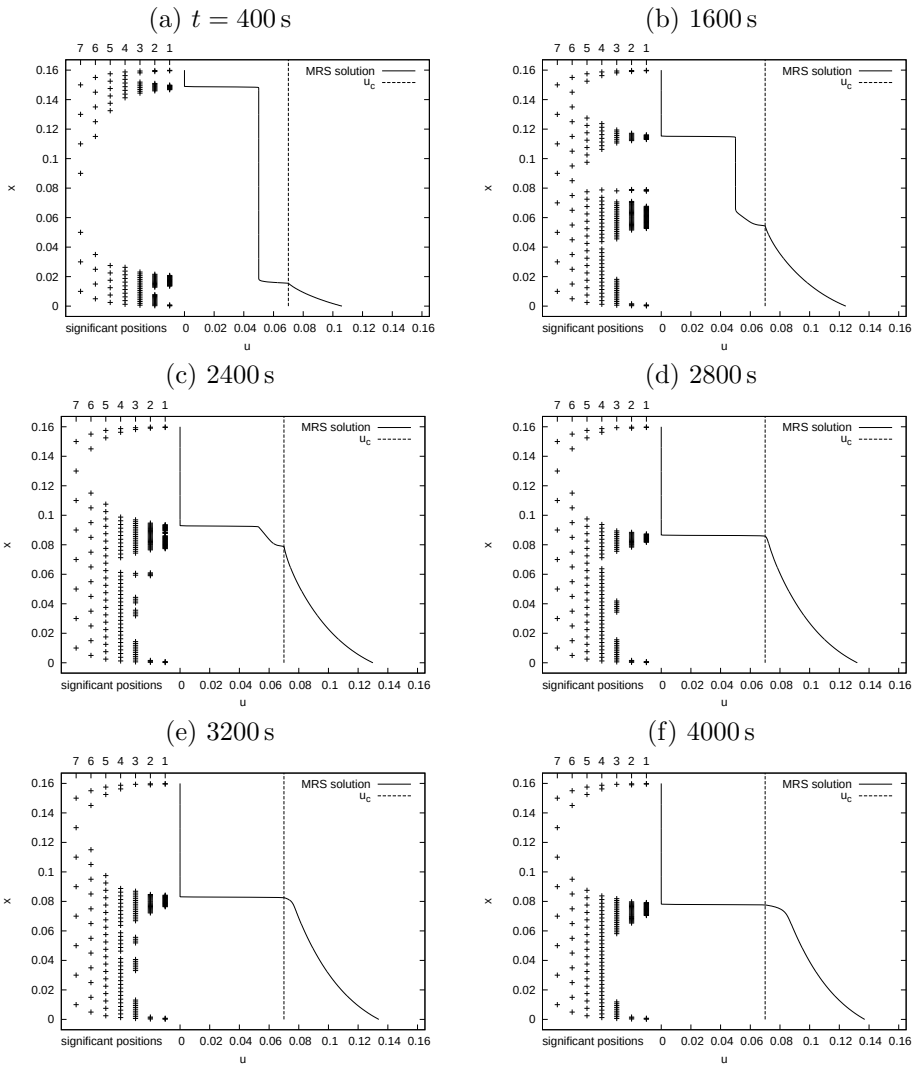

FIGURE 1. Numerical solution to the batch settling problem (Example 1) including significant positions of the wavelet coefficients.

4. Numerical results

4.1. Sedimentation-consolidation model (Example 1). As in [**4**] and other papers, we consider a suspension characterized by the function $f(u)$ given by (3.1) with $v_\infty = 2.7 \times 10^{-4}\,\mathrm{m/s}$, $C = 21.5$ and $u_{\max} = 0.5$, while the function $\sigma_e(u)$ is given by (3.2) with $\sigma_0 = 1.2\,\mathrm{Pa}$, $u_c = 0.07$ and $\beta = 5$. The remaining parameters are

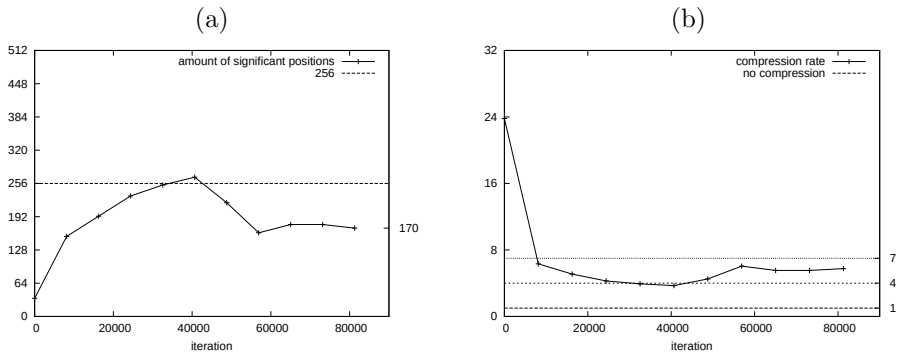

FIGURE 2. Number of significant wavelet coefficients and compression rate per iteration for Example 1.

$\Delta_\varrho = 1660\,\mathrm{kg/m^3}$ and $g = 9.81\,\mathrm{m/s^2}$. Note that for (3.1) with $\beta \in \mathbb{N}$, the function $A(u)$ has an explicit closed-form representation [**7**].

In Example 1, we consider an initially homogeneous suspension of concentration $u_0 \equiv 0.05$ in a column of depth $L = 0.16\,\mathrm{m}$. Figure 1 presents the solution at six different times. Here the finest multiresolution level is set to $N_0 = 2^{10}$, and the coarsest level to $N_{L_c} = 2^3$. The threshold parameter $\varepsilon_1 = 5.0 \times 10^{-8}$ is chosen constant at the first level of the multiresolution scheme, and the strategy for the remaining levels is $\varepsilon_k = 2\varepsilon_{k-1}$.

Example 1 involves zero-flux boundary conditions and the formation of a steady-state solution with a stationary type-change interface (the sediment level). For those points near the boundaries for which the central stencil of interpolation crosses the boundary (left or right), we change to a non-central stencil for the wavelet predictor and the flux calculation. The ENO interpolator always needs a greater amount of points around the position to be interpolated, so the function near the boundaries has to be extrapolated. We used the parameters CFL $= 0.085$, $\Delta t = 0.0491898\,\mathrm{h}$, $\Delta x = 0.00015625\,\mathrm{m} = 0.16\,\mathrm{m}/N_0$ and a final time $t = 4000\,\mathrm{s}$. The CPU time for this simulation was 200.4 min (user time) against 926.1 min when all fluxes are calculated on the fine grid without multiresolution.

Figure 1 also displays the grid positions of the significant wavelet coefficients of the solution. The marked positions are the current elements of the set $\tilde{\mathcal{D}}^n$ at which the flux and degenerate diffusion terms are evaluated explicitly. Unmarked positions correspond to coefficients that have been set to zero due to the thresholding operation, and where the flux and diffusion terms have been obtained by a simple cubic interpolation. Note that the finest of the eight levels involved is represented by the plotted solution, so that significant positions are marked for the remaining seven levels. Figure 1 illustrates how the scheme concentrates significant multiresolution coefficients near the downwards propagating shock separating the solution values zero and 0.05 (Figures 1 (a) and (b)), as well as near the parabolic-hyperbolic type change interface and near the boundary of the computational domain.

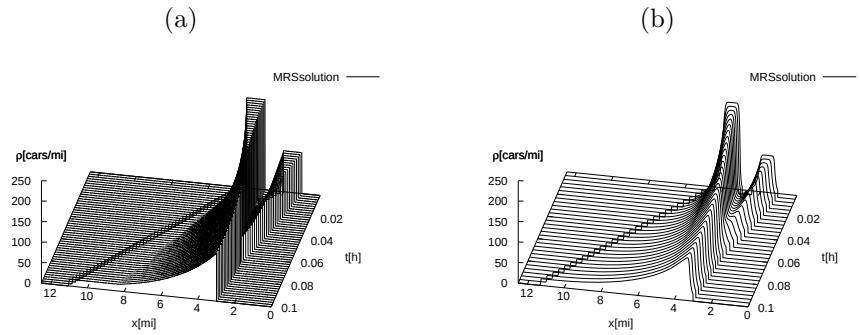

FIGURE 3. Solution to the traffic flow problem with two initial traffic jams: (a) kinematic model (LWR model), (b) diffusively corrected kinematic wave model (DCKWM) (Example 2).

Figure 2 shows the number of significant wavelet coefficients of the solution in each time step of the simulation and the corresponding compression rate (or efficiency) $N_0/\#\tilde{\mathcal{D}}^n$. When this rate equals one, there is no compression, and all grid positions are associated to significant coefficients. On the other hand, if $\#\tilde{\mathcal{D}}^n = 2^{L_c}$, then the maximum compression rate is achieved, and only function values on the coarsest level are sufficient to represent the function. This simulation starts from a very high compression rate, since the initial solution is constant all over the domain, having a discontinuity near the boundary. As time evolves, the solution changes rapidly, and through the multiresolution analysis, this variation of the smoothness of the function is recognized and translated into variation of the density of significant positions.

4.2. Traffic flow on an unbounded highway (Example 2). We consider the traffic model outlined in Section 3.2, and choose the velocity function and model parameters according to [**8, 19**]. The velocity function is given by (3.3) with $u_{\max} = 220\,\text{cars/mi}$, $C = \text{e}/7 = 0.38833$ and $v_{\max} = 70\,\text{mph}$, $u_{\text{c}} = 16.7512\,\text{cars/mi}$, so that

$$f(u) = \begin{cases} v_{\max} u & \text{for } 0 \leqslant u \leqslant u_{\text{c}}, \\ v_{\max}(\text{e}/7) u \ln(u_{\max}/u) & \text{for } u_{\text{c}} < u \leqslant u_{\max}, \\ 0 & \text{otherwise.} \end{cases} \tag{4.1}$$

We simulate the traffic density on an infinite road with the initial datum

$$u_0(x) = \begin{cases} 100\,\text{cars/mi} & \text{for } 1\,\text{mi} \leqslant x \leqslant 2\,\text{mi}, \\ 220\,\text{cars/mi} & \text{for } 3\,\text{mi} \leqslant x \leqslant 4\,\text{mi}, \\ 0 & \text{otherwise.} \end{cases} \tag{4.2}$$

We choose in (3.5) the parameters $a = 0.1\,g$, where g is the acceleration of gravity in $\text{mi}/(\text{h})^2$, $\tau = 2\,\text{s} = 0.000\bar{5}\,\text{h}$ and $L_{\min} = 0.05\,\text{mi}$.

Figure 3 (b) shows a three-dimensional plot of the solution, while Figure 4 presents the solution at four different times, where $N_0 = 2^{12}$, $\Delta x = 0.0048828125\,\text{mi}$, CFL =

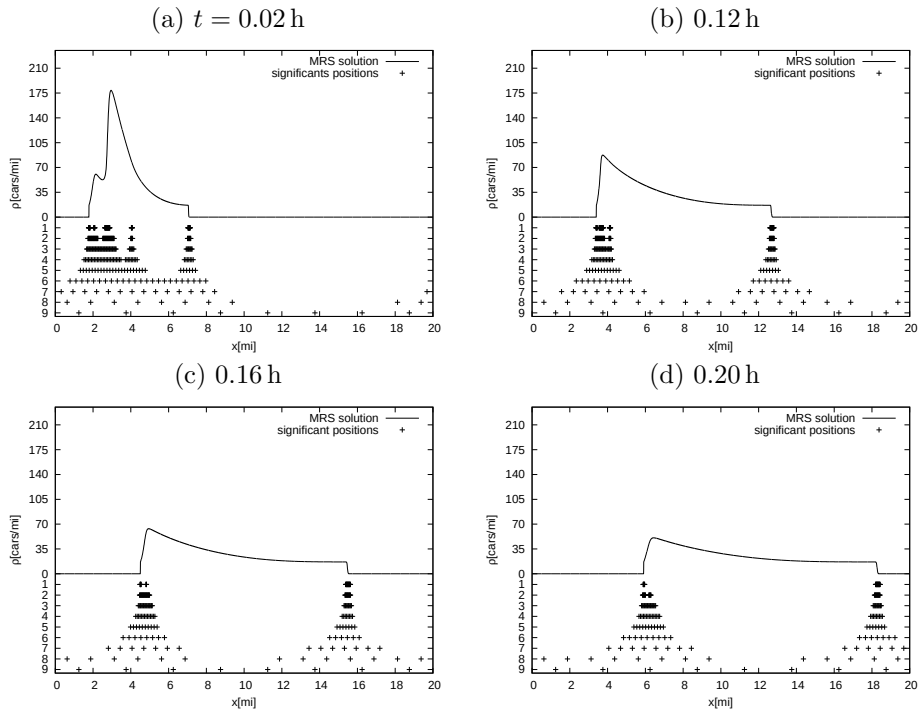

FIGURE 4. Numerical solution to the diffusively corrected traffic model (Example 2).

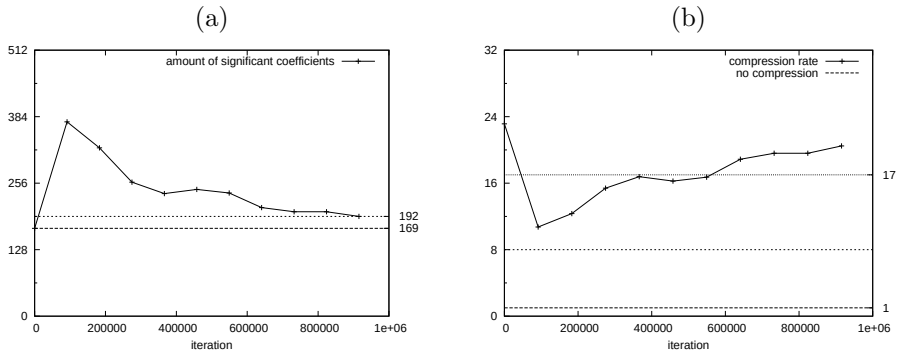

FIGURE 5. Number of significant coefficients and compression rate for the diffusively corrected traffic model (Example 2).

0.15 and $\Delta t = 2.18503946 \times 10^{-7}\,\mathrm{h}$. The CPU time for this simulation with multiresolution is 232.0 min. For a fine grid with $N_0 = 2^{11}$ points, the CPU time was 70.9 min.

N_0	$\|u-\tilde{u}\|_1$	$\|u-\tilde{u}\|_2$	$\|u-\tilde{u}\|_1/\|\tilde{u}\|_1$	$\|u-\tilde{u}\|_2/\|\tilde{u}\|_2$
	Simulated time $t = 0.01$ h			
2^7	1.35064719	5.89854274	0.09074661	0.14754827
2^8	0.54180785	1.76455705	0.03347226	0.04043202
2^9	0.25082264	1.40798155	0.01546539	0.03197256
2^{10}	0.13863086	0.48188979	0.00870690	0.01109847
2^{11}	0.09071482	0.44432536	0.00569469	0.01023377
	Simulated time $t = 0.1$ h			
2^7	1.15667976	6.74435950	0.07771442	0.24656450
2^8	0.32952242	1.29621014	0.02035751	0.04342227
2^9	0.29745421	1.90386338	0.01834063	0.06362897
2^{10}	0.11705983	0.55845444	0.00735210	0.01900646
2^{11}	0.09585902	0.70851873	0.00601762	0.02409528

TABLE 1. Errors for Example 2, measured at two simulated times, and referred to a fine grid solution with $N_0 = 2^{13}$.

In the case without multiresolution and the same fine scale, the CPU time is 698.5 min. We employed the tolerance $\varepsilon_1 = 5.1 \times 10^{-5}$. The results per iteration for compression rate and the number of significant wavelet coefficients are shown in Figure 5. Table 1 displays the errors between the reference solution and the multiresolution solution.

We observe that all significant positions are concentrated near the moving parabolic-hyperbolic type change interfacees. Between these interfaces, the solution varies smoothly. We observe in Figures 4 (c) and (d) that even though the solution is not constant between these interfaces, there exists a segment on which the solution is represented by the coefficients of the coarsest level only. The behaviour of the solution allows for high compression rates, as seen in Figure 5.

Acknowledgements

RB and MS acknowledge support by the Sonderforschungsbereich 404 at the University of Stuttgart, Germany, by Fondecyt projects 1050728, 1030718 and 7050230, Fondap in Applied Mathematics, and DAAD/Conicyt Alechile project. AK has been supported by FAPERGS, Brazil, by the ARD project 0306981, and FONDAP Program in Applied Mathematics (Project No. 15000001).

References

[1] S. Berres, R. Bürger, K.H. Karlsen and E.M. Tory, Strongly degenerate parabolic-hyperbolic systems modeling polydisperse sedimentation with compression, *SIAM J. Appl. Math.* **64** (2003), 41–80.

[2] B.L. Bihari and A. Harten, Application of generalized wavelets: a multiresolution scheme, *J. Comp. Appl. Math.* **61** (1995), 275–321.

[3] B.L. Bihari and A. Harten, Multiresolution schemes for the numerical solution of 2-D conservation laws I, *SIAM J. Sci. Comput.* **18** (1997), 315–354.

[4] R. Bürger, A. Coronel and M. Sepúlveda, On an upwind difference scheme for strongly degenerate parabolic equations modelling the settling of suspensions in centrifuges and non-cylindrical vessels, *Appl. Numer. Math.* **56** (2006), 1397–1417.

[5] R. Bürger, A. Coronel and M. Sepúlveda, A semi-implicit monotone difference scheme for an initial-boundary value problem of a strongly degenerate parabolic equation modelling sedimentation-consolidation processes, *Math. Comp.* **75** (2006), 91–112.

[6] R. Bürger, S. Evje and K.H. Karlsen, On strongly degenerate convection-diffusion problems modeling sedimentation-consolidation processes, *J. Math. Anal. Appl.* **247** (2000), 517–556.

[7] R. Bürger and K.H. Karlsen, On some upwind schemes for the phenomenological sedimentation-consolidation model, *J. Eng. Math.* **41** (2001) 145–166.

[8] R. Bürger and K.H. Karlsen, On a diffusively corrected kinematic-wave traffic model with changing road surface conditions, *Math. Models Meth. Appl. Sci.* **13** (2003), 1767–1799.

[9] R. Bürger, A. Kozakevicius and M. Sepúlveda, Multiresolution schemes for strongly degenerate parabolic equations in one space dimension, *Numer. Meth. Partial Diff. Eqns.*, to appear.

[10] G. Chiavassa and R. Donat, Point value multiscale algorithms for 2D compressive flows, *SIAM J. Sci. Comput.* **23** (2001), 805–823.

[11] A. Cohen, S.M. Kaber, S. Müller and M. Postel, Fully adaptive multiresolution finite volume schemes for conservation laws, *Math. Comp.* **72** (2001), 183–225.

[12] W. Dahmen, B. Gottschlich-Müller and S. Müller, Multiresolution schemes for conservation laws, *Numer. Math.* **88** (2001), 399–443.

[13] M.S. Espedal and K.H. Karlsen, Numerical solution of reservoir flow models based on large time step operator splitting methods. In: M.S. Espedal, A. Fasano and A. Mikelić (Eds.), Filtration in Porous Media and Industrial Application, Lecture Notes in Mathematics vol. 1734, Springer-Verlag, Berlin, 9–77, 2000.

[14] A. Harten, Adaptive multiresolution schemes for shock computations, *J. Comp. Phys.* **115** (1994), 319–338.

[15] A. Harten, Multiresolution algorithms for the numerical solution of hyperbolic conservation laws, *Comm. Pure Appl. Math.* **48** (1995), 1305–1342.

[16] A. Harten, Multiresolution representation of data: a general framework, *SIAM J. Numer. Anal.* **33** (1996), 1205–1256.

[17] A.J. Kozakevicius, Wavelets interpolatórias como ferramenta na resolução adaptativa de EDPs hiperbólicas, PhD Thesis, IME, Universidade de São Paulo, Brazil, 2002.

[18] M.J. Lighthill and G.B. Whitham, On kinematic waves. II. A theory of traffic flow on long crowded roads, *Proc. Roy. Soc. London Ser. A* **229** (1955), 317–345.

[19] P. Nelson, Traveling-wave solutions of the diffusively corrected kinematic-wave model, *Math. Comp. Modelling* **35** (2002), 561–579.

[20] P.I. Richards, Shock waves on the highway, *Oper. Res.* **4** (1956), 42–51.

[21] O. Roussel, K. Schneider, A. Tsigulin and H. Bockhorn, A conservative fully adaptive multiresolution algorithm for parabolic PDEs, *J. Comp. Phys.* **188** (2003), 493–523.

[22] C. Shu, Essentially non-oscillatory and weighted essentially non-oscillatory schemes for hyperbolic conservation laws. In: B. Cockburn, C. Johnson, C.-W. Shu and E. Tadmor, Advanced Numerical Approximation of Nonlinear Hyperbolic Equations (A. Quarteroni, Ed.), Lecture Notes in Mathematics vol. 1697, Springer-Verlag, Berlin (1998), 325–432.

Received 28 04 2006, revised 31 05 2006

[A]Departamento de Ingeniería Matemática,
Facultad de Ciencias Físicas y Matemáticas, Universidad de Concepción,
Casilla 160-C, Concepción, Chile.
E-mail address: rburger@ing-mat.udec.cl, mauricio@ing-mat.udec.cl

[B]Departamento de Matemática-CCNE-UFSM,
Santa Maria, Brazil,
Faixa de Camobi, km 9, Campus Universitário,
Santa Maria, RS, CEP 97105-900, Brazil.
E-mail address: alicek@smail.ufsm.br